Structural Engineering and Mechanics, Vol. 42, No. 1 (2012) 73-93
DOI: http://dx.doi.org/10.12989/sem.2012.42.1.073

Effect of compressible membrane's nonlinear stress-strain behavior on spiral case structure

Qi-Ling Zhang*[1] and He-Gao Wu[2a]

[1]*Changjiang River Scientific Research Institute, 430010 Wuhan, Hubei, China*
[2]*State Key Laboratory of Water Resources and Hydropower Engineering Science, Wuhan University, 430072 Wuhan, Hubei, China*

(Received October 14, 2011, Revised February 22, 2012, Accepted February 28, 2012)

Abstract. With an active structural involvement in spiral case structure (SCS) that is always the design and research focus of hydroelectric power plant (HPP), the compressible membrane sandwiched between steel spiral case and surrounding reinforced concrete was often assumed to be linear elastic material in conventional design analysis of SCS. Unfortunately considerable previous studies have proved that the foam material serving as membrane exhibits essentially nonlinear mechanical behavior. In order to clarify the effect of membrane (foam) material's nonlinear stress-strain behavior on SCS, this work performed a case study on SCS with a compressible membrane using the ABAQUS code after a sound calibration of the employed constitutive model describing foam material. In view of the successful capture of fitted stress-strain curve of test by the FEM program, we recommend an application and dissemination of the simulation technique employed in this work for membrane material description to structural designers of SCS. Even more important, the case study argues that taking into account the nonlinear stress-strain response of membrane material in loading process is definitely essential. However, we hold it unnecessary to consider the membrane material's hysteresis and additionally, employment of nonlinear elastic model for membrane material description is adequate to the structural design of SCS. Understanding and accepting these concepts will help to analyze and predict the structural performance of SCS more accurately in design effort.

Keywords: spiral case structure; compressible membrane; foam material; nonlinear stress-strain behavior; hydroelectric power plant

1. Introduction

With a complex shape and withstanding a high internal water pressure, spiral case structure (SCS) in a hydroelectric power plant (HPP) is always the design and research focus. For medium and high head plants, SCS is made of steel plate embedded in surrounding mass concrete. U.S. Army Corps of Engineers (1995) have suggested two commonly used methods of embedment of steel spiral cases in concrete, under an unwatered condition or a pressurized condition. When being embedded in concrete in an unwatered condition, it is suggested that the top portion of the spiral case should

*Corresponding author, Ph.D., E-mail: Liam1982@163.com
[a]Professor

be covered with a compressible membrane to ensure that the spiral case liner resists internal water pressure by ring tension, with only a small load being transmitted into the surrounding concrete. However, in real-world application, a minority of spiral cases were actually embedded in concrete under an unwatered condition without a compressible membrane covering.

The early structural researches on SCS were often carried out on some inaccurate assumptions. Aronson *et al*. (1985) presented a numerical calculation of spiral case for its nonlinear deformation under internal water pressure, with the surrounding concrete simulated as a Winkler elastic basis. Kalkani (1995) used SAP-IV finite element method (FEM) program to determine the expected displacements and stresses in the surrounding concrete of SCS, but unfortunately, the internal water pressure was ignored.

With a rapid hydroelectric development in many developing countries in recent years, intense attention has been given to the static and dynamic structural characteristics of SCS in HPP, considering multiple factors including construction procedures (Cui and Su 2007), crack propagation and effect (Wu *et al*. 2007, Tian *et al*. 2008), FEM modeling range effect (Zhang and Wu 2009, Zhang *et al*. 2009), fluctuating pressure excitation (Zhang and Zhang 2009) and seismic response (Ma and Zhang 2010). Most of the recent researches focused on NO.15 SCS of the Three Gorges Project (TGP) in China, which, as we know, is the world's largest power station in terms of installed capacity (22500 MW) and plays an extremely important role in the power grid system. The steel spiral case of TGP NO.15 SCS is embedded in concrete in an unwatered condition, with a small portion of steel spiral case's top covered with a compressible membrane, which was nevertheless ignored in FEM analysis (Tian *et al*. 2008, Zhang and Zhang 2009, Ma and Zhang 2010) for modeling convenience. With regard to few FEM studies (Wu *et al*. 2007, Zhang and Wu 2009) considering the compressible membrane, the membrane was assumed to be linear elastic material.

As suggested by U.S. Army Corps of Engineers (1995), polyvinylchloride (PVC) foam and polyurethane (PU) foam are acceptable material serving as the compressible membrane. Due to various operation modes of HPP, SCS is subjected to repeated and variable internal water pressure, which causes the cyclic compressions of membrane. Considerable testing and numerical studies (Hawkins *et al*. 2005, Fischer *et al*. 2009, Rizov 2009) dealing with mechanical properties of PVC and PU have proved that both materials exhibit essentially nonlinear mechanical behavior. Particularly, the softening phenomenon, generally known as the Mullins effect (Mullins 1969) considering rubbers, was observed (Krishnaswamy and Beatty 2000, Shen *et al*. 2001) in polymer foams under cyclic loading and unloading. The above works indicate that the idealized simplification of compressible membrane as linear elastic material in FEM analysis is likely to educe a coarse result and therefore, the practical applicability of the result obtained is limited, which has attracted our attention.

With the motivation to explore the effect of compressible membrane's nonlinear stress-strain behavior on SCS, we perform a representative FEM analysis of SCS with a compressible membrane, before which a brief introduction of SCS in structural terms and an outline of the role played by membrane are firstly presented. We use a nonlinear constitutive model to explicitly describe the nonlinear stress-strain behavior of membrane on the basis of a series of open test data. Concerning FEM analysis, the reliability and practicability of used computer program are of great importance. Research work on nonlinear constitutive modeling of foam is currently under active development. The latest achievement (Ogden and Roxburgh 1999) in this field is promptly included in the ABAQUS finite element program. Both static (Rizov 2009) and dynamic (Gilchrist and Mills

2001) ABAQUS-based FEM analyses simulating the nonlinear mechanical behavior of polymer foams show a practical performance of the program and the numerical analysis results demonstrate good agreement with experimental data. By coincidence, the ABAQUS code is frequently used for static (Wu *et al*. 2007, Zhang *et al*. 2009) and dynamic (Zhang and Zhang 2009, Ma and Zhang 2010) structural analysis of SCS with a good reliability. Therefore, the FEM analysis in this work is carried out on the basis of the ABAQUS code, which is particularly suitable for treating the structural analysis of SCS with a compressible polymer foam membrane. Before the case study, as it should be, the foam constitutive model is calibrated by comparing the program predicted behavior with the open test data to verify the accuracy of the applied finite element program.

2. Brief introduction of SCS with membrane

2.1 General description of SCS

As mentioned before, SCS for medium and high head plants can be classified as a distinctive type of steel-lined reinforced concrete structure. The steel lining designed as a housing to provide uniform water intake around the entire circumference of the distributor and keep the major part of the turbine mechanism apart from the water, is made of a number of steel plates with welded longitudinal and circumferential joints under strict quality control. The "*c*" cross section of a spiral case narrows at a constant rate downstream. The "*c*" sections of spiral case requiring field welding are as a rule buttwelded to skirt plates which have aforehand been shop-welded to the stay ring in position. A representative completed spiral case is as shown in Fig. 1.

After the assembly and installation of steel spiral case, a mesh reinforcement composed of both circumferential and longitudinal steel bars is arranged close to the steel lining, followed by the surrounding mass concrete placement. The steel spiral case, stay ring and surrounding reinforced concrete together compose SCS.

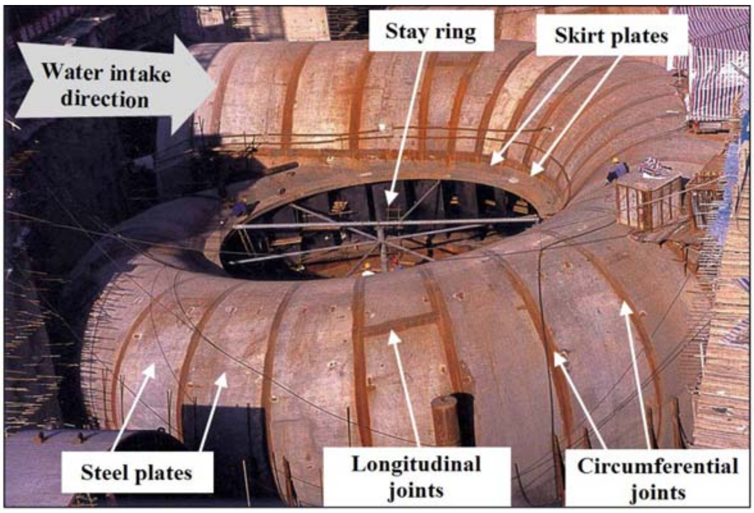

Fig. 1 Realistic display of completed spiral case

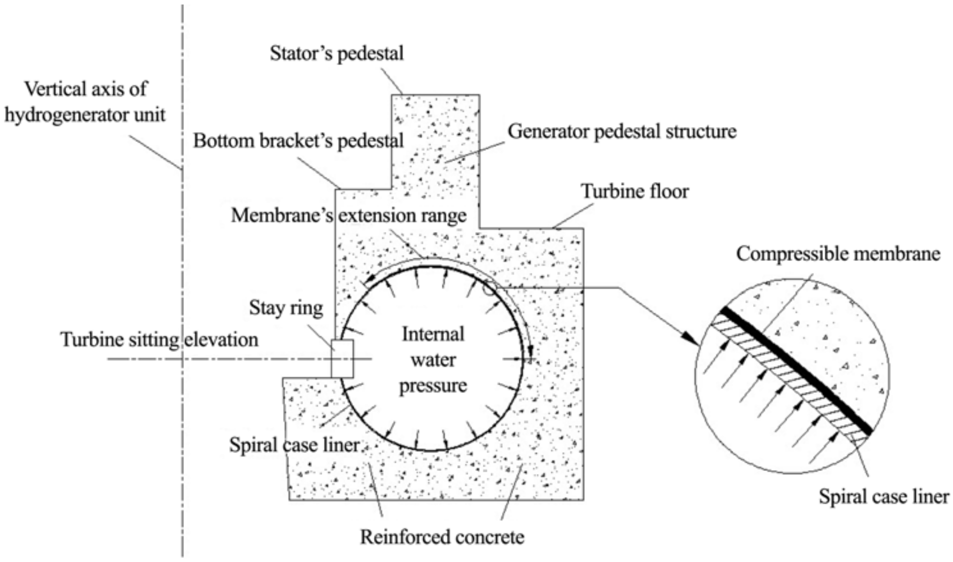

Fig. 2 Representative "*c*" cross section of SCS

2.2 Membrane's role in SCS

The compressible membrane consisting of sheets of polymer foam material adhered to the top exterior surface of spiral case liner ensures most internal water pressure acting on steel lining resisted by the lining itself, since the membrane with low modulus of compression provides a space of weak reaction for the expansion of spiral case. SCS with a compressible membrane virtually resembles a sandwich structure, in which the compression-dominated membrane plays the role of core sandwiched between steel spiral case and surrounding reinforced concrete, as illustrated in Fig. 2.

Even with a compressible membrane sandwiched between steel lining and surrounding concrete, the internal water pressure is actually jointly resisted by steel lining and surrounding concrete. At the same time, the membrane's structural involvement in SCS radically affects the joint stressing of spiral case and surrounding concrete together with the sliding behavior between them. With respect to the joint stressing, the covering membrane greatly increases the bearing participation by steel lining. Moreover, because of the weak reaction on steel lining's expansion by membrane and the partial covered area, under circumferentially quasi-uniform internal water pressure, the steel lining slides towards the membrane's extension range along circumference. This sliding behavior intensifies the pressure-bearing by steel lining to a higher degree (Yu *et al*. 2009).

In brief, the compressible membrane absolutely has a strong structural influence on SCS, concerning membrane's mechanical properties and extension range.

3. Compression test of membrane material

3.1 Material and test procedure

PU cork material manufactured by Xi'an Forest Products Chemical Plant (Xi'an, China) is finding wide and increasing employment as compressible membrane in SCS in China's HPP, such as Longyangxia (1280 MW, 1988), Lijiaxia (2000 MW, 1995), Gongboxia (1500 MW, 2003), Zipingpu (760 MW, 2004), Pengshui (1750 MW, 2006), Laxiwa (4200 MW, 2007), etc. The open compression test data supplied by Gan (2010) were referenced to assess the quality of ABAQUS-predicted membrane's mechanical behavior.

The nominal density of this PU cork is 240 kg/m^3. Cylindrical specimens of 61.8 mm in diameter were cut with a thickness of 30 mm. The compression test was carried out in a triple combination fixing instrument after a calibration. The specimens were compressed in a pressure cell with an inside diameter of 61.8 mm, which means the compression was in lateral confinement. The specimens were cycled 20 times in compression under pressure control. The maximum pressure was 0.8 MPa, with a loading/unloading gradation of 0.2 MPa. A pre-load of 0.0125 MPa for a sufficient contact was specified for compression test. A rest period of 5 min between gradations ensured a sufficient compressive deformation of specimens.

3.2 Test results and discussion

Fig. 3 shows the test stress-strain curves for loading and unloading cycles 1, 2, 10, 11, 19 and 20, respectively. Permanent strain at the end of each cycle is exhibited in Fig. 4.

As one can see in Fig. 3, the material tested exhibits generally nonlinear stress-strain response, with an increasing compression modulus accompanied by loading growth. The loading/unloading cycles do not occur along a single curve, and there is some amount of hysteresis, which is

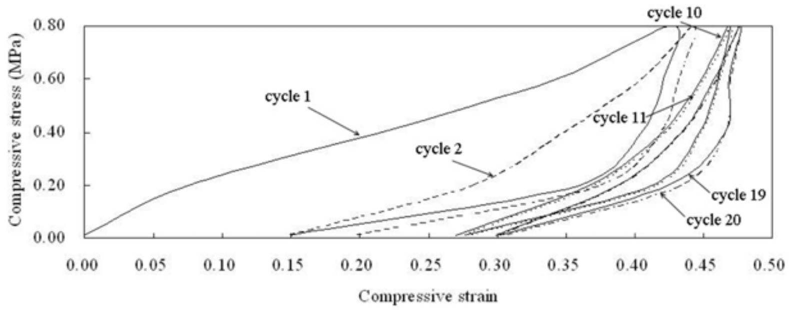

Fig. 3 Compression test stress-strain curves

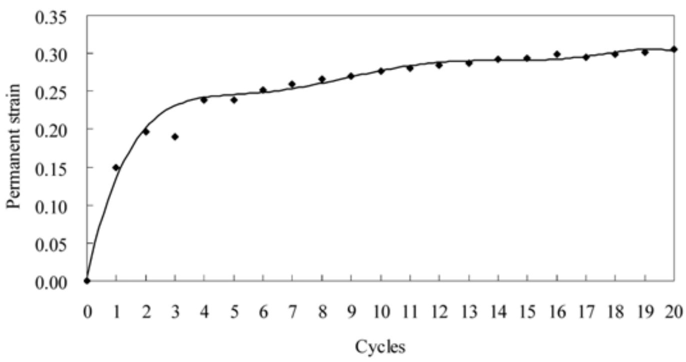

Fig. 4 Permanent strain versus cycles

especially remarkable in the initial few cycles and decreases with increasing number of cycles. Softening occurs quickly within the first few cycles, however, appears to stabilize after a number of cycles. This behavior is typical of strain induced softening of polymers in general.

Fig. 4 indicates that there is some amount of permanent set upon removal of the applied load. The data show evidence of progressive and irreversible damage with repeated cycling of compression. It can also be observed from the fitted curve that permanent set increases distinctly during the first 4 cycles, then more slowly for further cycles. Ultimately, the permanent set is approaching a steady state, with an approximate strain of 0.3 after 20 compression cycles.

In general, the material's compression mechanical behavior for different loading/unloading cycles is unique and cannot be retraced. However, for all that, after a number of compression cycles, the material is asymptotically approaching a steady state with a practically constant stress-strain curve. For HPP structural design purpose, a unique value of compression modulus is usually adopted as a key design parameter. Thus the stress-strain curve obtained on specimens without cycles of precompression is of little significance to determine compression modulus. The value of compression modulus determined after "conditioning" cycles of precompression is undoubtedly more reasonable and of more practical use.

With the purpose of obtaining quasi-steady stress-strain response of the tested material, the relative stress-strain curve of cycle 20 is fitted in Fig. 5, supposing the deformed state after previous 19 compression cycles to be initial condition. The loading linear elastic behavior is limited to relatively low values of compressive strain less than 0.1. Following the initial linear elastic phase, the curve slope gradually increases showing strain-hardening owing to material densification. On unloading, a stress-softened material curve lying below the loading curve is traced out. It is worthwhile to highlight that stress-softening phenomenon markedly dominates the early unloading phase before compressive stress decreases to 0.2 MPa. In succession the unloading curve follows a practically linear elastic relationship and ultimately approaches the starting point of loading curve with a negligible permanent strain of 0.004.

It should be specified that for the same material, the membrane's compression degree constantly varies with internal water pressure, steel lining's thickness, membrane's thickness and surrounding concrete's size of different SCS. Accordingly, by reason of the limited linear elastic behavior phase and the gradual increase in compression stiffness during loading seen in Fig. 5, it is none the less slightly difficult to determine a unique value of compression modulus for design purpose even

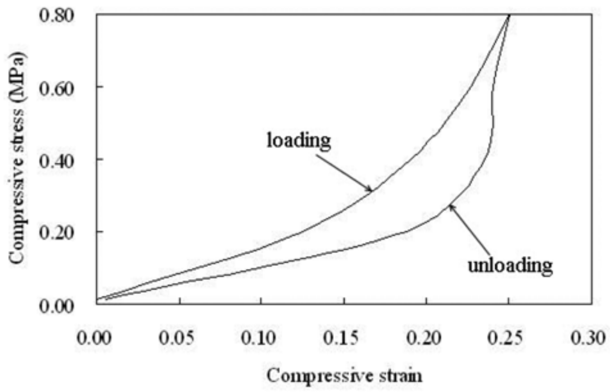

Fig. 5 Relative stress-strain curve of cycle 20

though the specimens have been under cycles of precompression. Furthermore, along with different operation modes of HPP, the internal water pressure regularly rises or falls, which causes repeated compressions of membrane. In such circumstances, the nonlinear stress-strain behavior of membrane material has an imaginable effect on SCS in structural terms, which is the focus of this work.

4. Calibration of program

For the selection of suitable foam constitutive model and material coefficients for numerical work, important criterion is the ability to capture the stress-strain curve of test. For this purpose, the ABAQUS software was used to reproduce the cycle 20 of compression test in Section 3, ignoring the permanent strain of 0.004. The numerical model was based on the dimension and geometry of tested specimens. Owing to the axial symmetry of cylindrical specimen, only a radial cross section was modeled, as shown in Fig. 6.

The model, composed of 176 elements and 204 nodes, was meshed using 4-node bilinear axisymmetric solid elements (CAX4). The left, right and bottom boundaries were restrained in normal direction to respectively simulate symmetry axis of specimen, lateral confinement and pressure cell bottom, in company with the top surface loaded by uniform pressure. It should be stated that the thickness of modeled specimen is 21 mm on the assumption that the progressive permanent deformation in pace with repeated cycling of compression has terminated with a strain of 0.3.

For the material description of PU cork, the *HYPERFOAM option, which optionally allows the specification of energy dissipation and stress-softening effect, was employed to define the primary behavior of tested material obtained from the monotonic loading curve in Fig. 5. In addition, the *MULLINS EFFECT option was used to model energy dissipation in foam material. In this way, the ABAQUS code can establish the stress-strain behavior of stabilized cycle in Fig. 5, of which the quality should be assessed by comparing the prediction of material behavior against the test data. Both of the two aforementioned options require a set of constants for material description, and fortunately, test data can be provided to the program using the *UNIAXIAL TEST DATA option

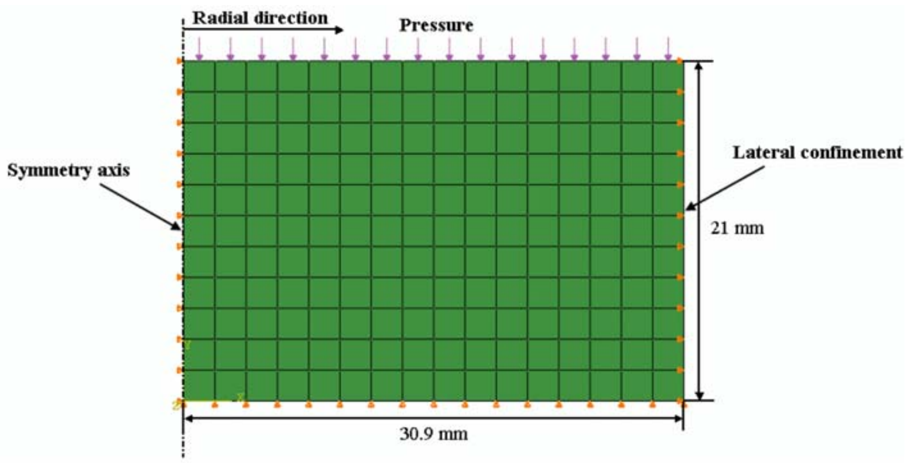

Fig. 6 FEM model of specimen

for calculating the material constants.

Due to the insufficient loading/unloading gradations of compression test, much more fitted test data are needed for accuracy and smoothness of material description. For this reason, each original loading/unloading gradation of 0.2 MPa was equally divided into 10 stages and the corresponding compressive strain was fitted by the following equation ignoring the pre-load of 0.0125 MPa

$$\varepsilon = c_1\sigma^4 + c_2\sigma^3 + c_3\sigma^2 + c_4\sigma \quad (1)$$

The coefficients c_i for the loading and unloading paths were respectively determined using a trendline fitting method (Microsoft Office Excel 2003), given in Table 1.

When the *HYPERFOAM option is used, an optional parameter N equaling to the order of strain energy potential should be set. In the following fitting work, both $N = 2$ and $N = 3$ parameters were assessed. Considering the buckling of foam cell walls commonly does not result in any significant lateral deformation after cycles of precompression treatment with the specimen, the material's Poisson's ratio was assumed to be effectively zero.

The rounded loading/unloading process was supposed to be in linear progress lasting 20 s, and the pressure reached the peak value of 0.8 MPa at 10 s corresponding to a loading/unloading rate of 0.08 MPa/s. In order to make the dynamic analysis normally performed and as well, reduce the inertia effect to a minimum, the material's density was assigned a small value of 10^{-15} kg/m^3. The output was written at a time interval of 0.25 s equating to a loading/unloading gradation of 0.02 MPa, aiming at getting a one-to-one correspondence between numerical calculation results and fitted test data. Comparison of the numerical calculation results with the original and fitted test data is shown in Fig. 7.

It is apparent that the polynomial expression (Eq. (1)) captures the original test data with high

Table 1 Coefficients in Eq. (1) for loading and unloading paths

Path	c_1	c_2	c_3	c_4
Loading	−0.2612	0.9103	−1.2073	0.8303
Unloading	−1.3804	3.7160	−3.5981	1.5204

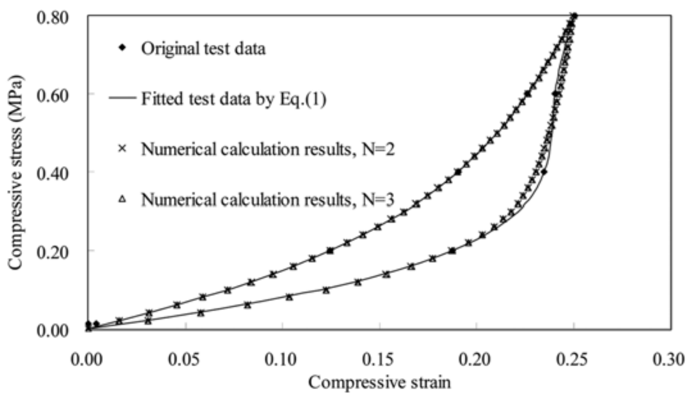

Fig. 7 Comparison of numerical calculation results with test data

accuracy and describes a reasonable and functional loading/unloading curve for being provided to the program. The numerical calculation results for both values of N match the loading fitted test data extremely well, but nevertheless do not accurately reproduce the sharp descent stage of early unloading fitted curve until compressive stress decreases to 0.2 MPa.

Besides predicting the stress-strain curve, the ABAQUS software can also provide an approach intended for modeling energy dissipation in foam material as history-type output. The area enclosed by the hysteresis loop of stress-strain curve corresponds to the specific dissipated energy for a cycle given by

$$\Delta E = \int_0^{\varepsilon_{\max}} (\sigma_{ld}(\varepsilon) - \sigma_{ul}(\varepsilon))d\varepsilon = \int_0^{\sigma_{\max}} (\varepsilon_{ul}(\sigma) - \varepsilon_{ld}(\sigma))d\sigma \tag{2}$$

where $\sigma_{\max}$, $\varepsilon_{\max}$ are the maximum stress and strain respectively, σ_{ld}, ε_{ld} are the stress and strain on loading curve respectively, and σ_{ul}, ε_{ul} are the stress and strain on unloading curve respectively. With Eq. (2), Eq. (1) and coefficients in Table 1, the specific dissipated energy ΔE for fitted cycle can be obtained equaling to 0.0268 MJ/m^3. By multiplying ΔE, area (30 cm^2) and thickness (2.1 cm) of the modeled specimen, the dissipated energy for a fitted cycle can easily be worked out equaling to 1.688 J. By comparison, the predicted values of dissipated energy for $N = 2$ and $N = 3$ models are respectively 1.674 J and 1.675 J. In view of the comparison, the program's ability for predicting energy dissipation per cycle is satisfactory.

On the whole, in view of the above-mentioned assessment, employment of the *HYPERFOAM option and the *MULLINS EFFECT option in conjunction with the *UNIAXIAL TEST DATA option is effective and reliable in describing the mechanical behavior of PU cork in regard to stress-strain response and energy dissipation of a stabilized loading/unloading cycle when uniaxial compression test data are used in fitting the material constants. It is worth to mention that the value assignment of optional parameter $N = 2$ or $N = 3$ produces little effect on the numerical calculation results for this work.

5. Case study on SCS in Laxiwa HPP

5.1 Project profile of Laxiwa HPP

Located in Qinghai province, China, the Laxiwa HPP which features the largest installed capacity on the main stream of the Yellow River, China's second longest river, is a key source of power supply in the national west-to-east power transmission channel with a unit capacity of 700 MW, totaling to a capacity of 4200 MW. All of the 6 hydrogenerator units are located in underground powerhouse on the right bank.

The main generator room is divided into 6 blocks by contraction joints, with one hydrogenerator unit located in each block. The block has a width (upstream-downstream dimensions) of 26.8 m and a length (left-right bank dimensions) of 34 m. The diameter of spiral case's water intake is 6.8 m. The spiral case designed to withstand a maximum internal water pressure (maximum headwater plus water hammer) of 2.76 MPa is embedded in concrete in an unwatered condition covered with a 20 mm-thick PU cork membrane. The plan view of SCS at the elevation of turbine sitting is briefly shown in Fig. 8.

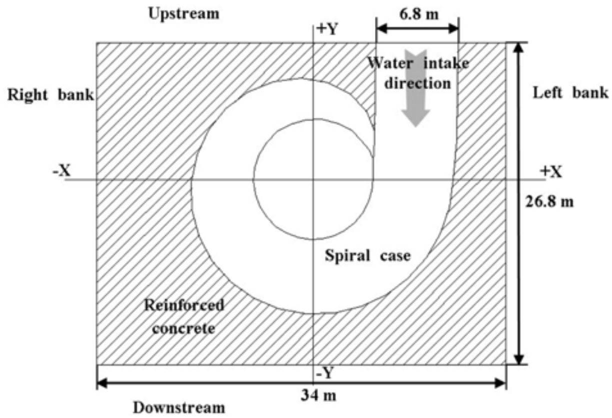

Fig. 8 Plan view of SCS at the elevation of turbine sitting

5.2 FEM model

Notwithstanding the narrowing of "*c*" cross section of spiral case downstream, structural analysis of SCS can be roughly considered as an axisymmetric problem in view of the fact that structural performance of different "*c*" cross sections is localized primarily influenced by spiral case's radius and surrounding concrete's size. In practical design work, usually, several representative "*c*" cross sections thereby are respectively treated and the representative design schemes are applied to adjacent cross sections. Yu *et al*. (2009) performed an intensive investigation on the influencing factors of reinforcement calculation for SCS with a compressible membrane and confirmed the feasibility of simplifying SCS as axisymmetric structure in preliminary design work. Therefore in this work, to maximize efficiency and minimize computational cost, 2 representative cross sections of both $+X$ and $-X$ coordinate axis (Fig. 8) were modeled, as shown in Fig. 9. The mesh of concrete close to spiral case liner is condensed with the element edge length of about 0.2 m due to the expected material damage in this zone. The $+X$ model is composed of 3292 nodes and 3216

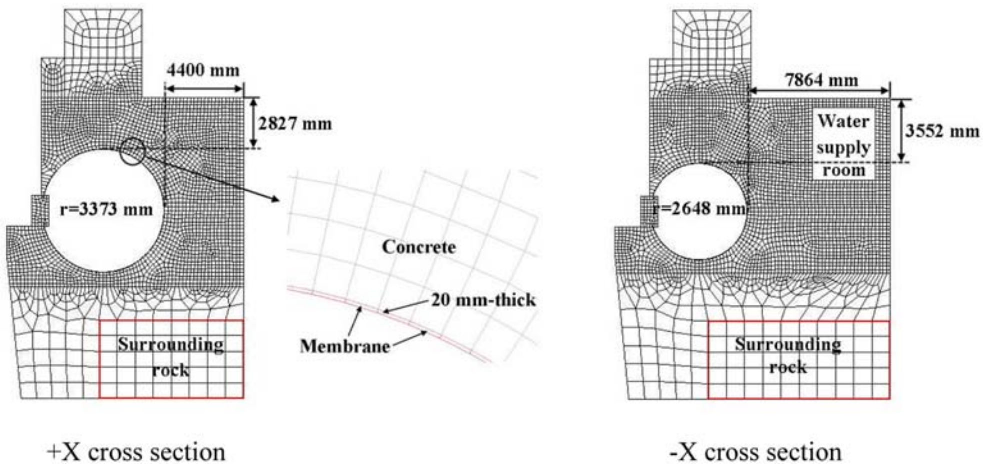

Fig. 9 Axisymmetric FEM model of representative cross sections

elements, while the $-X$ model is composed of 3561 nodes and 3447 elements correspondingly.

The 4-node bilinear axisymmetric solid element (CAX4) was used to model the concrete, compressible membrane, surrounding rock and vertically extending vanes of stay ring. However, on account of the spaced-discontinuity of stay vanes, both elastic modulus and density of CAX4 elements modeling the stay vanes were equivalently reduced so as to allow for an equivalence of vertical stiffness and dead weight.

The 2-node linear axisymmetric shell element (SAX1) was used to represent the two vertically spaced-apart ring members of stay ring, spiral case liner, draft tube liner and cylindrical inside steel

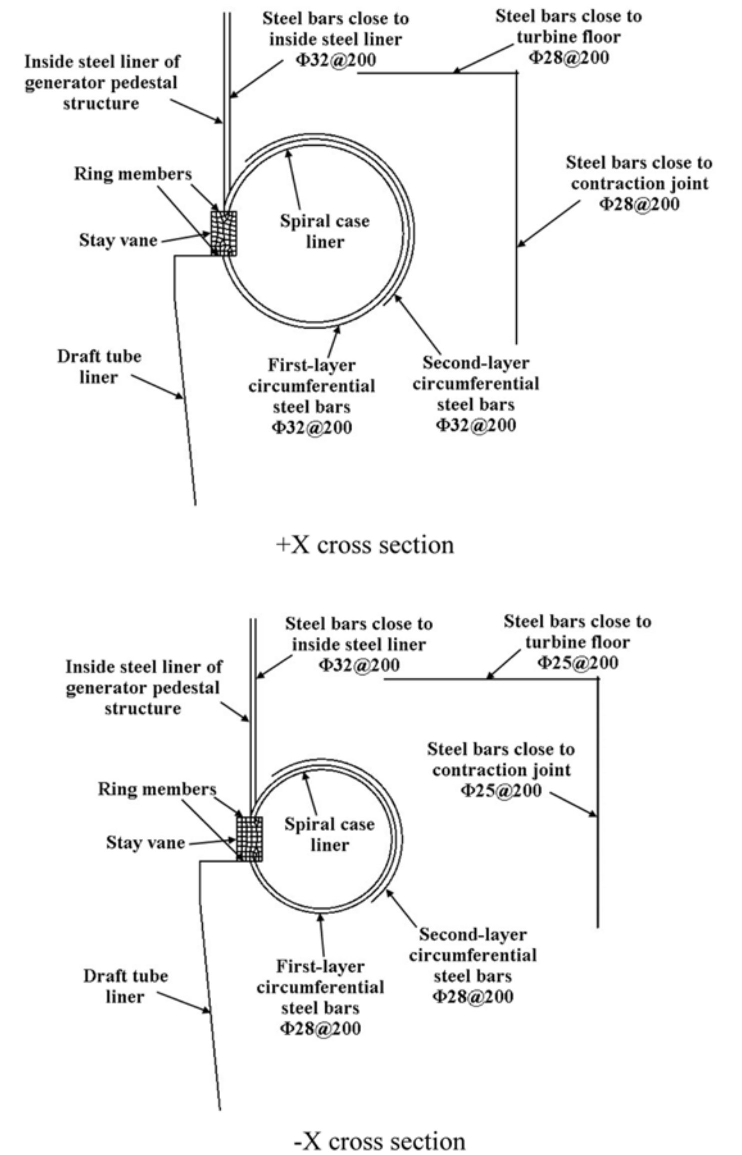

Fig. 10 Steel structure in representative cross sections

liner of generator pedestal structure. The steel bars arranged close to various steel liners or surface of concrete structure were also represented by SAX1 in consideration of the close reinforcement arrangement. On this assumption, the thickness of SAX1 modeling mesh reinforcement was determined allowing the shell and the modeled steel bars are equal in cross-sectional area per unit length along the extension of mesh reinforcement.

The steel structure in SCS including stay ring, various steel liners and steel bars is shown in detail in Fig. 10. All the elements modeling steel bars are embedded in the concrete element group by means of employing the *EMBEDDED ELEMENT option, which slaves the translational degrees of freedom of the embedded nodes to the interpolated values of the corresponding degrees of freedom of the host (concrete) elements. Though the embedded elements (SAX1) have a rotational degree of freedom in the plane, the rotation is not constrained by the embedding.

In view of the fact that the foam material serving as compressible membrane is attached to the spiral case liner with an adhesive (U.S. Army Corps of Engineers 1995), the solid elements (CAX4) representing compressible membrane share the common nodes of the shell elements (SAX1) representing spiral case liner at the corresponding spatial locations. The aforementioned two groups of elements as a whole were specified as an element-based surface by using the *SURFACE option for contact simulation. In the same way, another element-based surface was defined on the internal circular surface of concrete elements. After definition of the two overlapped surfaces, the *CONTACT PAIR option was used to enforce the expected contact and sliding action between spiral case liner and concrete, or between compressible membrane and concrete. In the definition of contact, the concrete surface was chosen as the master surface for the higher stiffness of surrounding concrete structure compared to that of spiral case liner. The augmented Lagrange method was chosen for enforcement of the contact constraint by using the *SURFACE BEHAVIOR option including the AUGMENTED LAGRANGE parameter.

5.3 Calculation parameters

In accordance with the design data, friction coefficient in the analysis was defined as 0.2. The basic material parameters are presented in Table 2. The shell thicknesses of SAX1 modeling various

Table 2 Basic material parameters

	Concrete	Steel	Steel for stay vanes	Surrounding rock
Young's modulus (MPa)	28000	206000	28644	10000
Poisson's ratio	0.167	0.3	0.3	0.27
Mass density (kg/m^3)	2500	7800	1080	2700

Table 3 Shell thicknesses of SAX1 (mm)

	Ring members	Spiral case liner	Inside steel liner of generator pedestal structure	Draft tube liner	Steel bars
+*X* model	180	97 (Skirt plates), 65, 44	20	20	4.02 (Φ32), 3.08 (Φ28)
−*X* model	180	77 (Skirt plates), 46, 35	20	20	4.02 (Φ32), 3.08 (Φ28), 2.45 (Φ25)

steel structures are listed in Table 3.

As common concrete is known for its high compressive strength and low tensile strength, the tension crack of concrete in SCS has received a great deal of attention these years (Wu *et al*. 2007, Tian *et al*. 2008, Zhang *et al*. 2009, Zhang and Zhang 2009, Ma and Zhang 2010), and the concrete damaged plasticity model in the ABAQUS code is extensively employed in describing the inelastic behavior and irreversible damage of concrete in SCS (Zhang *et al*. 2009, Zhang and Zhang 2009, Ma and Zhang 2010). This model based on the models proposed by Lubliner *et al.* (1989) and by Lee and Fenves (1998) aims to capture the effects of irreversible damage associated with the failure mechanisms that occur in concrete under fairly low confining pressures. Therefore, in this work the concrete damaged plasticity model was employed using the *CONCRETE DAMAGED PLASTICITY option. The *CONCRETE TENSION STIFFENING option was used to specify the postcracking behavior of concrete by entering the postfailure stress/cracking-strain relationship on the assumption that the material's tensile stress-strain response follows a linear elastic relationship until the value of the failure stress σ_{t0} is reached. The cracking strain ε_t^{ck} is defined as the total strain ε_t minus the elastic strain ε_t^{el} corresponding to the undamaged material; that is

$$\varepsilon_t^{ck} = \varepsilon_t - \varepsilon_t^{el} = \varepsilon_t - \frac{\sigma_t}{E_0} \tag{3}$$

where σ_t is the postfailure stress and E_0 is the initial (undamaged) Young's modulus of concrete. The stress-strain response adopted in this study is illustrated by Fig. 11. Seeing that the concrete surrounding spiral case is tension-dominated, which means the compressive stress of concrete in SCS hardly reaches compressive strength, an initial yield stress in compression and crushing strain 17 MPa and 0 were selected by using the *CONCRETE COMPRESSION HARDENING option, respectively, for the operating conditions under investigation.

The stiffness degradation caused by the microcracking process of concrete, which is difficult to represent with classical plasticity, was defined by way of using the *CONCRETE TENSION DAMAGE option. The tensile damage variable d_t characterizing stiffness degradation is defined as a tabular function of cracking strain ε_t^{ck}. Fig. 12 shows the $d_t - \varepsilon_t$ curve adopted in the present study.

In order to clarify the effect of compressible membrane's nonlinear stress-strain behavior on SCS, the majority of the work presented herein focuses on the selection of different mechanical models and parameters for describing compressible membrane material. Exactly as the conventional design analysis follows, a parametric approach was used by respectively assigning the compression

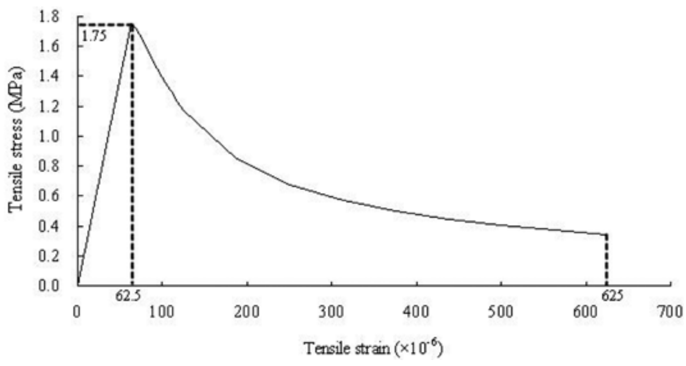

Fig. 11 Adopted stress-strain curve of concrete in tension

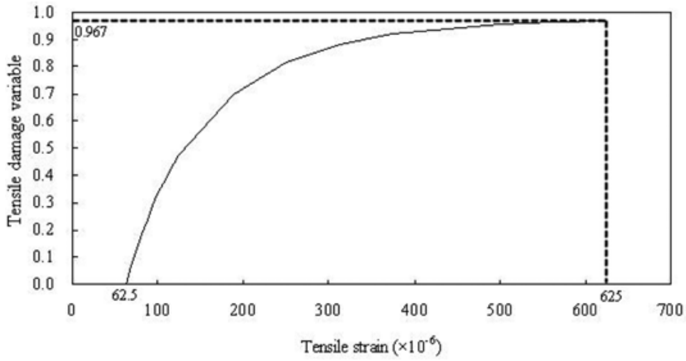

Fig. 12 Adopted $d_t - \varepsilon_t$ curve of concrete

Table 4 Summary of different material descriptions for membrane in 4 investigation schemes

	Scheme *A*	Scheme *B*	Scheme *C*	Scheme *D*
Mechanical model	Linear elastic	Linear elastic	Nonlinear elastic	Nonlinear inelastic
Stress-strain behavior	E_m = 2.10 MPa	E_m = 3.19 MPa	Loading curve in Fig. 5	Rounded loading/unloading curve in Fig. 5

modulus of membrane material E_m two different values on linear elastic assumption. Selection of the two values was based on the two different loading gradations of 0.4 MPa and 0.8 MPa in Fig. 5, educing 2.10 MPa and 3.19 MPa as membrane's compression modulus respectively. Besides assuming the membrane to be linear elastic material with two different values of compression modulus in routine analysis, a third investigation scheme was developed to allow for nonlinear elastic assumption, meaning that the loading/unloading process in Fig. 5 occurs along a single curve (loading curve) without the hysteresis loop. For this purpose of material description, only the *HYPERFOAM option was employed to define the loading process of foam material. The fourth ultimate investigation scheme was performed considering the rounded loading/unloading process by adopting the simulation technique upon completion of the program validation, as described in Section 4. The different mechanical models and parameters for describing membrane material adopted in the forementioned 4 investigation schemes are briefly summarized in Table 4. It should be noted that the optional parameter *N* for the *HYPERFOAM option was set equaling to 2 in Scheme *C* and *D.* The membrane material's mass density was defined as 340 kg/m^3, about 10/7 times the original value considering the material's permanent strain of 0.3.

5.4 Loads and boundary conditions

Model bottom boundary, together with the lateral (right) boundary of surrounding rock (Fig. 9), was assumed to be fixed in normal direction, whereas the lateral (right) boundary of concrete structure was idealized as a free surface taking contraction joints into account.

A rounded loading/unloading process simulation was considered by prescribing a variation in rising/falling internal water pressure in multiple static load steps. The maximum pressure ($P_{\max}$) of 2.76 MPa was applied at 0.276 MPa increments/decrements to generate various structural

Table 5 Live loads (MPa)

	On turbine floor	On stator's pedestal*	On bottom bracket's pedestal**
Pressure value	0.03	0.098	1.809

Note: *The inside and outside radiuses of stator's pedestal are 6.1 m and 7.8 m respectively.
**The inside and outside radiuses of bottom bracket's pedestal are 4.8 m and 5.2 m respectively.

performances of SCS; thus 21 load steps in all were defined, with the pressure value maximizing in the 11th step. All the static constant-loads, including dead weight of structure and various assumed uniform live loads caused by weights of control equipments, turbine and generator over turbine floor, stator's pedestal and bottom bracket's pedestal (Fig. 2), were applied in the first step and remained unchanged in the subsequent 20 steps. The values of different live loads provided by the manufacturers are collected in Table 5.

5.5 Results and discussion

5.5.1 Compressive strain of membrane

Considering the membrane's strong structural influence on SCS, as described in Section 2, a comparison of the representative compressive strain of membrane versus internal water pressure is illustrated in Fig. 13 for all of the investigation schemes. The membrane's compression degree virtually distributes uniformly along membrane's circumferential extension range (Fig. 2) other than at the both ends. Accordingly, the compressive strain of midpoint of membrane's extension range is deemed to be representative herein.

In general, the progress tendencies of compressive strain of the 2 models analyzed are similar as expected owing to the essential structural comparability of the 2 models (Fig. 9). For all of the schemes considered, the calculated strain is basically within the range of 0.05-0.25, which is in the main consistent with strain range of the test data adopted (Fig. 7) and confirms its applicability for Scheme *C* and *D*. The calculated strain in the first step is approximately or somewhat greater than 0.05 indicating an initial compression state of membrane caused by weights of superstructure, equipments and machines. For Scheme *A*, *B* and *C*, the progress curves all reveal a fundamental symmetry at corresponding pressure stages of ascending and descending branches, but such a symmetry is not found for Scheme *D*. The asymmetry of progress curves for Scheme *D* confirms the expectation that the membrane material of SCS may show a hysteresis phenomenon supposing the internal water pressure falls from a higher level for operating requirement of HPP.

The progress curves for Scheme *A* and *B* both exhibit a practically linear response owing to the adopted linear elastic model for describing membrane material in the 2 schemes. The smaller value assigned to E_m in Scheme *A* leads to a higher compression degree of membrane, when compared with that in Scheme *B*.

In contrast, the expected nonlinear process appears to be apparent for Scheme *C* and *D*, as a result of the adoption of nonlinear stress-strain response for membrane material. The ascending branches for Scheme *C* and *D* coincide with each other, yet this coincidence does not occur for the descending branches. The flatter descending branches for Scheme *D* should be attributed to the marked stress-softening phenomenon dominating the early unloading phase in Fig. 5.

The progress curves for Scheme *B* lie below those for Scheme *C* and *D* all along since E_m

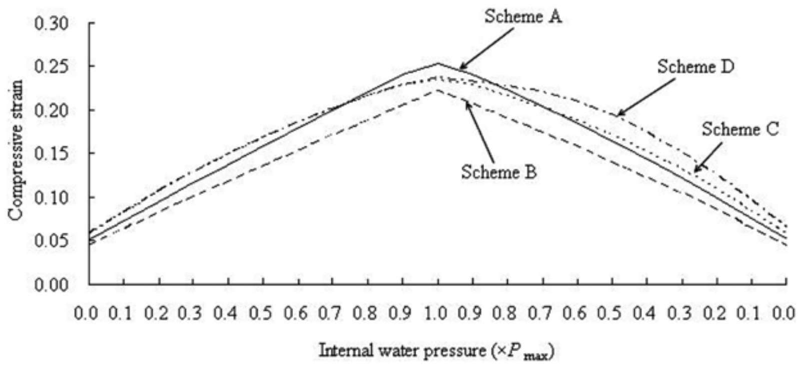

+X model

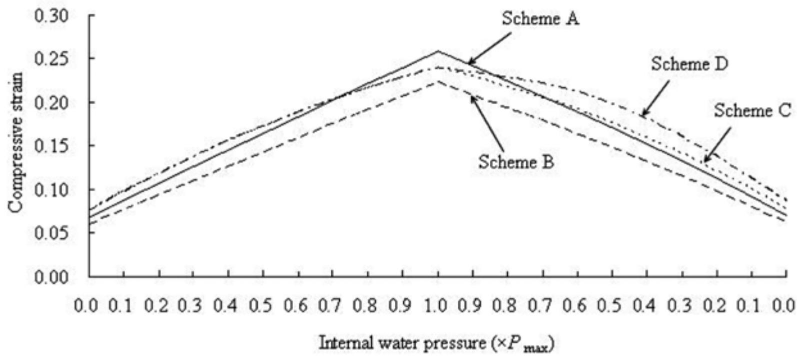

-X model

Fig. 13 Representative compressive strain of membrane versus internal water pressure

adopted for Scheme *B* was effectively over-valuated. In light of the gradual strain-hardening phenomenon of loading process in Fig. 5, obviously, the over-valuation is attributed to the extreme determination of the value of E_m based on the highest loading gradation of 0.8 MPa. As for Scheme *A*, in the ascending phase of progress curves, the leading segments are progressing below those for Scheme *C* and *D* and then above, with intersections occurring at the strain level of approximately 0.2. This strain level on loading curve in Fig. 5 generally corresponds to the loading gradation of 0.4 MPa, just based on which the value of E_m for Scheme *A* was determined. Similar intersections understandably occur likewise in the descending phase of progress curves.

From a structural design standpoint, making an attempt to determine a unique value of compression modulus for membrane material description based upon the material's nonlinear stress-strain curve, however on linear elastic assumption as is customary in conventional practice, is definitely incapable of capturing the nonlinear compression response as internal water pressure varies, and may bring about an imaginably coarse result of structural analysis of SCS. Expected inaccuracy cannot be satisfactorily avoided even though a nonlinear elastic model is employed, when taking the regular operation-required unloading of internal water pressure into consideration.

Table 6 Representative damage of concrete structure and tensile stress in steel bar

		Scheme *A*	Scheme *B*	Scheme *C*	Scheme *D*
+*X* model	d_t of concrete	0.20	0.94	0.27	0.27
	σ_t in steel bar (MPa)	7.52	13.38	8.59	8.59
−*X* model	d_t of concrete	0	0	0	0
	σ_t in steel bar (MPa)	3.01	3.94	3.41	3.41

5.5.2 Damage of concrete structure

To further investigate the influence of compressible membrane's nonlinear stress-strain behavior on SCS, representative damage of concrete structure d_t and corresponding maximum tensile stress in steel bar σ_t in all of the investigation schemes are presented in Table 6 for comparison. Concrete at the elevation of turbine floor adjacent to generator pedestal structure has been demonstrated to damage or crack easily (Wu *et al*. 2007, Zhang *et al*. 2009) and due to its long-term exposure to external environment, the local damage or crack of concrete greatly influences the structural durability of SCS. In addition, it is common knowledge that crack width of concrete depends on many quantities among which tensile stress in steel bar plays an important role. For the above reasons, the corner joint of turbine floor and generator pedestal structure is considered to be representative herein.

Because of the smaller spiral case's radius and relatively larger surrounding concrete's size of −*X* model (Fig. 9), concrete at the corner joint of turbine floor and generator pedestal structure does not damage in all of the 4 schemes and hence difference in σ_t for the 4 schemes is negligible from the standpoint of structural design of SCS.

Conversely for +*X* model, concrete damage at the corner joint is apparent and this finding is in agreement with those reported by Wu *et al*. (2007) and Zhang *et al*. (2009), even based upon different case studies. The earlier comparison of compressive strain of membrane for the 4 schemes indicates a smaller expansion deformation of spiral case for Scheme *B* that results in a weaker bearing participation by steel lining and accordingly, a higher proportion of internal water pressure transmitted into surrounding concrete. Consequently d_t of Scheme *B* for +*X* model is dramatically greater than that of other schemes. Due to the greater concrete damage, σ_t of Scheme *B* is also relatively greater for maintaining composite action of reinforced concrete structure that requires load transfer from concrete to steel bar. Furthermore it is understandable that d_t and σ_t of Scheme *A* are less than those of Scheme *C* and *D* considering the higher membrane's compression degree of Scheme *A* under the maximum internal water pressure (Fig. 13). It should be pointed out that d_t and σ_t of Scheme *C* and *D* are identical respectively on account of the same definition of loading process of membrane material for the 2 schemes.

According to the above analysis, potential arbitrariness of determining the value of membrane's compression modulus on linear elastic assumption may lead to conservative or excessive predictions of d_t and σ_t. To be exact, the customary way of determining membrane's compression modulus may bring about a risky or conservative design scheme for structural reinforcement of SCS. With a view to rational structural reinforcement, taking into account the nonlinear stress-strain response of membrane material in loading process is definitely essential but nevertheless similar consideration for membrane material in unloading process seems dispensable.

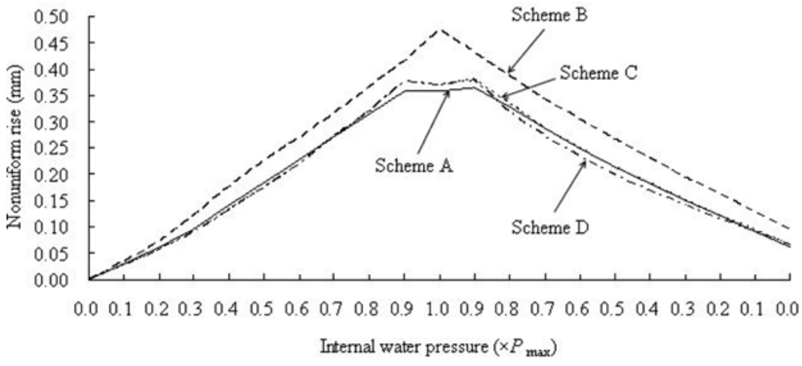

Bottom bracket's pedestal

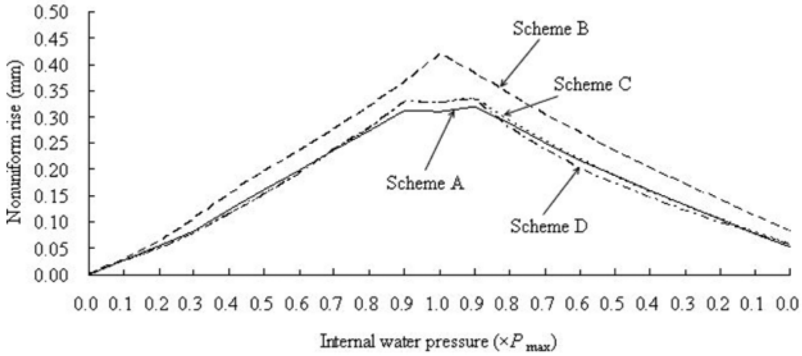

Stator's pedestal

Fig. 14 Nonuniform rise of generator pedestal structure between $+X$ and $-X$ cross sections versus internal water pressure

5.5.3 Nonuniform rise of generator pedestal structure

In the design of SCS, special attention is devoted to nonuniform rise of generator pedestal structure that is critical to the safe operation of hydrogenerator. In view of the fact that support bearings of hydrogenerator and stators have been positioned in a horizontal plane before water filling of SCS, the calculated initial settlement of generator pedestal structure in the first step caused by dead weight and weight of hydrogenerator set is ignored. In other words, the nonuniform rise caused solely by internal water pressure essentially influences the running performance of hydrogenerator. Fig. 14 illustrates the differential rise between $+X$ and $-X$ cross sections versus internal water pressure at bottom bracket's pedestal and stator's pedestal respectively, for all of the investigation schemes.

The progress tendencies of nonuniform rise at the two pedestals are on the whole reasonably similar. The nonuniform rises of bottom bracket's pedestal are superior to those of stator's, and considering the smaller inside radius of bottom bracket's pedestal, obviously, the former nonuniform rises for certain cause greater tilting of the pedestal plane. Because of the over-valuation of E_m

adopted for Scheme *B* that gives rise to an overestimated proportion of internal water pressure transmitted into surrounding concrete, as previously stated, the nonuniform rises for Scheme *B* are observably higher than those of other schemes. Interestingly it is observed, that practically linear increases of the nonuniform rises for Scheme *A*, *C* and *D* all unexpectedly terminate at the same loading gradation of $0.9P_{max}$. Whereafter, the curves simultaneously display a visible "platform" extending through to the unloading gradation of $0.9P_{max}$, and then show practically linear decrease. This unexpected "platform" phenomenon might be attributed to the sudden local damage of concrete adjacent to the lower ring member of stay ring under the maximum internal water pressure in $-X$ cross section for Scheme *A*, *C* and *D*. The local stiffness degradation of concrete in $-X$ cross section induces a higher rise rate, wherefore in the 11th step, the calculated increment of rise value in $-X$ cross section approximates that in $+X$ cross section. Consequently the nonuniform rises stop increasing in the 11th step and the aforementioned "platform" phenomenon arises. The "platforms" for Scheme *A* lie below those for Scheme *C* and *D* corresponding to the higher compression degree of membrane under the maximum internal water pressure for Scheme *A* (Fig. 13). For Scheme *C* and *D*, the noncoincidence occurs in the descending phase as expected, whereas the difference appears limited. In particular symmetry cannot be observed of curves for all of the schemes considered, with a certain amount of ultimate differential rise generated by the damage-caused irreversible plastic deformation of SCS.

The discussion presented above indicates that the hysteresis of membrane material exerts a minor influence on prediction of the nonuniform rise of generator pedestal structure in the design analysis of SCS. For this reason taking the membrane material's hysteresis into consideration is supposed to be unnecessary to the corresponding prediction in design effort. However, the nonlinear stress-strain response of membrane material in loading process should not be ignored.

6. Conclusions

This manuscript has carried out a case study on SCS with a compressible membrane on the basis of the ABAQUS code, to clarify the effect of membrane (foam) material's nonlinear stress-strain behavior on SCS, before which the employed constitutive model describing foam material was attentively calibrated. The FEM program, using uniaxial compression data for material description, successfully captures the fitted stress-strain curve of test with satisfactory accuracy. Thus it is reasonable to state that the simulation technique applied in this work for membrane material description is reliable and practical, and furthermore, similar application of the technique can be popularized in the further design analysis of SCS.

Even more important, the case study presented in this work argues that, since the customary way attempting to determine a unique value of membrane's compression modulus on linear elastic assumption fails to capture the membrane's nonlinear compression response as internal water pressure varies and as well due to the membrane's active structural involvement in SCS, taking into account the nonlinear stress-strain response of membrane material in loading process is definitely essential from a structural design standpoint. Despite the fact that inaccuracy of prediction for membrane's compression degree cannot be satisfactorily avoided without consideration of the membrane material's hysteresis in view of the regular operation-required unloading of internal water pressure, the inaccuracy seems to produce no crucial influence on prediction of the damage of concrete structure and the nonuniform rise of generator pedestal structure in the design analysis of

SCS. Therefore we suggest that there is no need to consider the membrane material's hysteresis and employment of nonlinear elastic model for membrane material description seems adequate to the structural design of SCS.

Acknowledgements

The authors express their thanks to Basic Scientific Research Operating Expenses of Central-level Public Academies and Institutes (Changjiang River Scientific Research Institute CKSF2012021/GC) and National Natural Science Foundation of China (51179141) for financial support.

References

Aronson, A.Ya., Bazhenov, V.A., Gotsulyak, E.A., Gulyaev, V.I. and Ogloblya, A.I. (1985), "Nonlinear deformation of shells of the volute chambers of hydraulic turbines in an elastic medium", *Strength Mater.*, **17**(4), 555-560.

Cui, J.H. and Su, H.D. (2007), "3-D FEM emulation computation on surrounding concrete of steel spiral case keeping internal pressure during construction", *Proceedings of International Symposium on Computational Mechanics*, Beijing, China, July.

Fischer, F., Lim, G.T., Handge, U.A. and Altstdt, V. (2009), "Numerical simulation of mechanical properties of cellular materials using computed tomography analysis", *J. Cell. Plast.*, **45**(5), 441-460.

Gan, Q.M. (2010), "Characteristic and influence factors analysis of compression modulus of polyurethane cork cushion material", *Water Power*, **36**(5), 82-84. (in Chinese)

Gilchrist, A. and Mills, N.J. (2001), "Impact deformation of rigid polymeric foams: Experiments and FEA modelling", *Int. J. Impact Eng.*, **25**(8), 767-786.

Hawkins, M.C., O'Toole, B. and Jackovich, D. (2005), "Cell morphology and mechanical properties of rigid polyurethane foam", *J. Cell. Plast.*, **41**(3), 267-285.

Kalkani, E.C. (1995), "Expected displacements and stresses in the encasing concrete of a Francis turbine scroll case", *Comput. Struct.*, **55**(4), 735-739.

Krishnaswamy, S. and Beatty, M.F. (2000), "The Mullins effect in compressible solids", *Int. J. Eng. Sci.*, **38**(13), 1397-1414.

Lee, J. and Fenves, G.L. (1998), "Plastic-damage model for cyclic loading of concrete structures", *J. Eng. Mech.*, **124**(8), 892-900.

Lubliner, J., Oliver, J., Oller, S. and Oate, E. (1989), "A plastic-damage model for concrete", *Int. J. Solids Struct.*, **25**(3), 299-326.

Ma, Z.Y. and Zhang, C.H. (2010), "Static and dynamic damage analysis of mass concrete in hydropower house of Three Gorges Project", *Trans. Tianjin Univ.*, **16**(6), 433-440.

Mullins, L. (1969), "Softening of rubber by deformation", *Rubber Chem. Technol.*, **42**(1), 339-362.

Ogden, R.W. and Roxburgh, D.G. (1999), "A pseudo-elastic model for the Mullins effect in filled rubber", *Proc. R. Soc. Lond. A*, **455**(1988), 2861-2877.

Rizov, V. (2009), "Indentation of foam-based polymer composite sandwich beams and panels under static loading", *J. Mater. Eng. Perform.*, **18**(4), 351-360.

Shen, Y., Golnaraghi, F. and Plumtree, A. (2001), "Modelling compressive cyclic stress-strain behaviour of structural foam", *Int. J. Fatigue*, **23**(6), 491-497.

Tian, Z.Q., Zhang, Y.L., Ma, Z.Y. and Chen, J. (2008), "Effect of concrete cracks on dynamic characteristics of powerhouse for giant-scale hydrostation", *Trans. Tianjin Univ.*, **14**(4), 307-312.

U.S. Army Corps of Engineers (1995), EM 1110-2-3001 Planning and Design of Hydroelectric Power Plant Structures, Department of the Army, Washington, DC.

Wu, H.G., Shen, Y. and Jiang, K.C. (2007), "Structural research on embedment of a bare deflated spiral case",

Wuhan Univ. J. Natural Sci., **12**(2), 311-316.
Yu, Y., Zhang, Q.L. and Wu, H.G. (2009), "Reinforcement calculation for spiral case embedded with cushion layer of hydropower station", *J. Tianjin Univ. Sci. Tech.*, **42**(8), 673-677. (in Chinese)
Zhang, C.H. and Zhang, Y.L. (2009), "Nonlinear dynamic analysis of the Three Gorge Project powerhouse excited by pressure fluctuation", *J. Zhejiang Univ. Sci. A*, **10**(9), 1231-1240.
Zhang, Q.L. and Wu, H.G. (2009), "Modal analysis of hydropower house by using finite element method", *Proceedings of 2009 Asia-Pacific Power and Energy Engineering Conference*, Wuhan, China, March.
Zhang, Q.L., Wu, H.G. and Yang, H.Q. (2009), "Effect of modeling range on structural analysis for powerhouse of hydroelectric power plant by FEM", *Trans. Tianjin Univ.*, **15**(5), 388-392.